Heavy Nuclei, from RHIC to the Cosmos

Spencer R. Klein[a]

[a]Lawrence Berkeley National Laboratory, Berkeley, CA, 94720, USA

Ultra-relativistic heavy ion collisions produce a high-temperature, thermalized system that may mimic the conditions present shortly after the big bang. This writeup will given an overview of early results from the Relativistic Heavy Ion Collider (RHIC), and discuss what we have learned about hot, strongly interacting nuclear systems. The thermal and chemical composition of the system will be discussed, along with observables that are sensitive to the early evolution of the system. I will also discuss the implications of the RHIC results for cosmic ray air showers.

1. Introduction

The Relativistic Heavy Ion Collider (RHIC) at Brookhaven National Laboratory (BNL) collides ultra-relativistic ions at energies up to 200 GeV per nucleon. The nucleon-nucleon reactions are energetic enough that perturbative QCD is expected to be able to describe much of the collision dynamics.

The goal of ultra-relativistic heavy ion collisions is to study the properties of matter at extremely high temperatures and/or densities, with an eye to mimicing the conditions present in the very early universe, $\approx 10\mu$s after the big bang. A specific goal is to look for the Quark-Gluon Plasma, a state of matter whereby the protons and neutrons in a nucleus 'dissolve', producing a gas of free quarks and gluons.

These collisions may also be similar to those produced when heavy-ion cosmic rays hit the atmosphere. In the target frame, RHIC projectile gold nuclei have a total energy of 4.3 PeV (20 TeV per nucleon), energetically reaching the knee of the cosmic ray spectrum.

Relativistic heavy ion collisions were initially studied at the Berkeley Bevatron, SIS and the Dubna Nuclotron[1]. More recently, there have been higher energy studies at the BNL AGS and the CERN SPS. The SPS data is often used as a lower-energy comparison point; the SPS collided lead on lead, at a center of mass energy of 17 GeV per nucleon. The earlier studies found several interesting phenomena. These include:

Anisotropic flow: Heavy ion collisions may be described at least partly in terms of fluid dynamics; the system shows fluidlike behavior[2].

Strangeness enhancement: Production of strange particles is several times larger than would be expected from superimposed *pp* collisions[3][4][5].

J/ψ suppression: Production of J/ψ particles is suppressed compared to the production of Drell-Yan dileptons[3][6].

The latter two observations have been proposed as signatures of the Quark Gluon Plasma. However, both phenomena might be due to normal hadronic interactions, with the additional strangeness produced in secondary reactions among the produced hadrons, and the J/ψ suppression due to interactions with the initial state nucleons and the other hadrons produced in the collision.

In low energy heavy ion collisions, the interacting baryons stop when the nuclei collide. As the collision energy increases, the nuclei gradually become transparent, the baryons retain some of their initial momentum, and the net baryon density of the produced system drops. At RHIC, the net baryon density at mid-rapidity (near the system center of mass) should be near zero.

This writeup will discuss heavy ion collisions at RHIC, starting with observables that probe thermal freezeout, such as the global event characteristics, system size, particle spectra, and non-

isotropic flow. Next, the composition at chemical freezeout will be discussed, followed by signatures of the early evolution, focusing on high p_T particles and charm production.

2. RHIC

RHIC is a 3.8 km circumference double-ring accelerator which can collide gold ions at center of mass energies of up to 200 GeV/nucleon at a luminosity of $2 \times 10^{26}/\mathrm{cm}^2/\mathrm{s}$, corresponding to about 1,500 hadronic collisions/sec. RHIC can also accelerate lighter ions. The maximum energy per nucleon depends on the charge to mass ratio; for protons, the maximum center of mass energy is 500 GeV. It also collides polarized protons, to study the spin structure of the nucleon. The luminosity depends on the species; for protons the luminosity can reach $1.4 \times 10^{31}/\mathrm{cm}^2/\mathrm{s}$, or about 700,000 hadronic interactions/sec.

In the year 2000, RHIC collided gold nuclei at an energy of 130 GeV/nucleon. Most of the results presented here are from this run. In 2001/2, RHIC collided gold nuclei at 200 GeV/nucleon, briefly reaching the design luminosity, and collided polarized protons, with up to 25% polarization. The long term program will include studies with lighter ions, gold-gold collisions at lower energies, and deuterium-gold and/or proton-gold collisions.

RHIC is instrumented with two large detectors, STAR and PHENIX, and two smaller experiments, BRAHMS and PHOBOS. A third small experiment, *pp*2*pp*, studies proton-proton elastic scattering[7]. The collaborations have very different strategies for studying ion collisions.

PHENIX is designed to look for relatively rare observables that are sensitive to the early phases of the collision, such as charmed hadrons, J/ψ and direct photons[8]. The detectors are optimized for particle identification, especially leptons and photons. PHENIX has a two-armed central spectrometer; each arm is instrumented with charged particle tracking, time-of-flight (TOF), a ring imaging Cherenkov counter (RICH), and electromagnetic calorimetry. Each arm covers a solid angle of 135 degrees in azimuth by 0.3 in pseudorapidity, where the pseudorapity $\eta = -\ln[\tan(\theta/2)]$, with θ the particle angle with respect to the beam axis. The center of mass is at $\eta = 0$. Forward and backward muon detectors cover $1.2 < |\eta| < 2.2$ for muons with momentum $p > 2$ GeV/c. Specialized triggers and a high rate DAQ system will collect large samples of the selected rare probes.

The Solenoidal Tracker at RHIC (STAR) is optimized to study hadrons over a very large solid angle, including multi-particle correlations, and measure global event characteristics[9].

STAR tracks charged particles with $\eta| < 1.5$ in a large time projection chamber (TPC) in a 5 kG solenoidal magnetic field. A silicon vertex detector covering $|\eta| < 1$ and two forward TPCs covering $2.5 < |\eta| < 4.0$ complete the tracking system. Strange particles like K_S, Λ, Ξ and Ω are detected by reconstructing secondary vertices. Energy loss in the TPCs and SVT and small TOF and RICH systems provide particle identification, along with an electromagnetic calorimeter. STAR records a great deal of information on each event, but can only record data from selected events at rate slower than PHENIX.

PHOBOS records charged and neutral particle production over most of phase space, up to $|\eta| < 5.4$, to search for anomalous event shapes[10]. It has two small charged particle spectrometers with TOF systems for particle identification.

BRAHMS is composed of precision central and forward spectrometers with tracking and particle identification, along with counters to measure charged multiplicity[11].

The 4 experiments include identical zero degree calorimeters (ZDCs) to measure forward neutrons from nuclear fragmentation[12]. The ZDCs are intended to provide a common method for luminosity and centrality (impact parameter) measurements, in order to facilitate comparisons between the four experiments.

3. Ultra-Peripheral Collisions

Before discussing central collisions, it is interesting to consider ultra-peripheral collisions (UPCs), interactions at large impact parameters b (minimum ion-ion separation) where only photonuclear and two-photon interactions are possi-

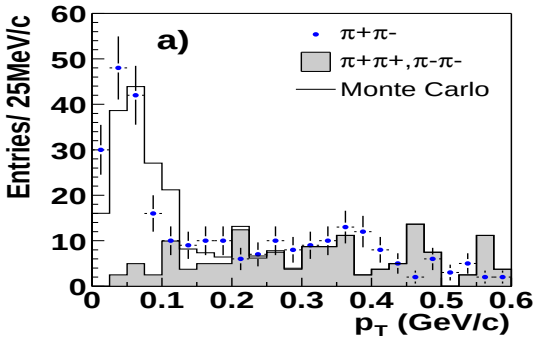

Figure 1. p_T spectrum of 2 track events observed at 130 GeV in STAR. The peak at low p_T is characteristic of coherent coupling to both nuclei, as expected for coherent ρ^0 photoproduction[18].

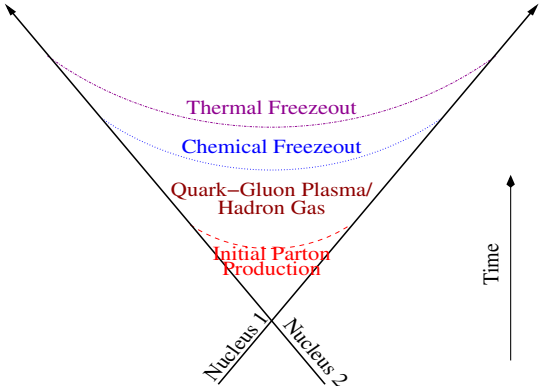

Figure 2. Schematic view of a heavy ion interaction, showing the different stages of the reaction.

ble. UPCs can probe a wide variety of physics[13], ranging from electrodynamics in very strong electromagnetic fields to meson spectroscopy to measurements of gluon shadowing in heavy nuclei to tests of quantum mechanics[14]. Photoproduction of heavy hadrons[15] and quarkonium[16] is sensitive to the gluon density in the nucleus, and hence to gluon shadowing.

At RHIC, mutual nuclear excitation (including both Coulombic and hadronic interactions) is used as a luminosity monitor[17]. The process has a large cross section, about 11 barns, and small backgrounds.

One easily observable UPC process is exclusive coherent photoproduction of vector mesons, $Au+Au \rightarrow Au+Au+\rho^0$. These events are characterized by an almost empty detector, containing only two tracks, with a total event transverse momentum $p_T < 2\hbar/R_A \approx 100$ MeV/c. The low p_T, characteristic of the coherent photon emission and scattering, is a distinctive signature, as data from STAR shows in Fig. 1. At 130 GeV, STAR measures $\sigma(Au+Au \rightarrow Au+Au+\rho^0) = 460 \pm 220 \pm 110$ mb[18], in agreement with theoretical predictions[19]. The ratio of ρ^0 to direct $\pi^+\pi^-$ production is consistent with that measured in γp interactions.

4. Hadronic Collisions

Hadronic collisions occur in several stages, as is shown in Fig. 2. The nucleons collide, and their partons interact. The produced particles interact and form hadrons (hadronize). As the interactions continue and the number of particles grows, the system expands and cools, When the average particle energy is low enough, inelastic hadron production stops, a transition known as chemical freezeout. Slightly later, the interparticle separation is large enough that even elastic interactions cease; this is thermal freezeout.

The key question in this picture is whether the produced particles interact as hadrons (i.e. a hadron gas) or as partons (i.e., a quark-gluon plasma). Partons produced in the initial interactions may remain free for long enough to interact with each other and equilibrate, forming a quark-gluon plasma. Or, they might immediately form hadrons (hadronize), and the interacting system will be a hadron gas. Or, they could initial interact as a quark-gluon plasma, and, then, as the system cools, hadronize to form a hadron gas.

Most of the theoretical guidance regarding the quark-gluon plasma comes from lattice gauge theory (LGT). Recent LGT calculations indicate that the phase transition between hadron gas and quark-gluon plasma, if it occurs, is weak (at

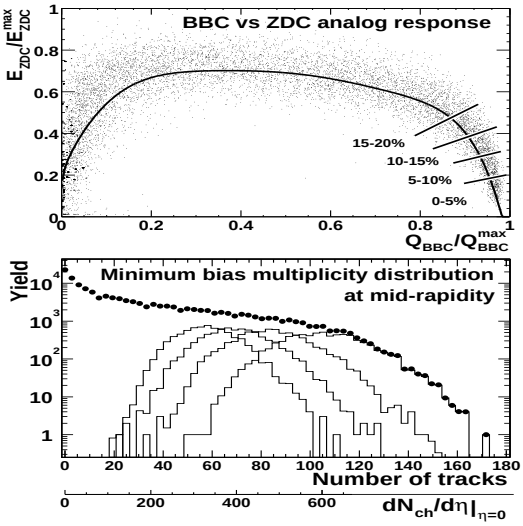

Figure 3. (a)Relationship between forward neutrons (ZDC energy) and charged multiplicity (the charge in the beam-beam counters, Q_{BBC}), as measured by the PHENIX collaboration at 130 GeV for 4 impact parameter bins. (b) The overall charged particle multiplicity, $d\sigma/dN_{ch}$ (solid dots), with calculations of the multiplicity distribution for the same 4 impact parameter bins. From Ref. [21].

least second order), and occurs at a temperature of 150-200 MeV and an energy density $\epsilon_c \approx 1$ GeV/fm^3[20]. This calculation is for an infinite medium with an infinite lifetime; edge effects and formation time are not considered. Although the expected system lifetime is only $\approx 10^{-23}$s, calculations indicate that equilibration occurs quickly, so a clear phase change is possible.

Although it is a key parameter in heavy ion collisions, the impact parameter b is not directly observable. We use two classes of observables to infer the impact parameter. The first is the number of forward (zero-degree) neutrons. These neutrons come from the non-interacting part of the nucleus. Enough energy propagates from the initial collision to dissociate the non-interacting part of the nuclei into neutrons, protons and small nuclear fragments. The other observables are sensitive to the number of interacting nucleons. Examples are the charged particle multiplicity or transverse energy. A model is necessary to relate these observables to the impact parameter. To avoid systematic uncertainties, events are often sorted by centrality (*i.e.* by charged multiplicity), and divided into classes, such as the 10% most central (those with the smallest impact parameter).

Figure 3 shows the relationship between the number of forward neutrons (measured in the ZDCs) and the charged multiplicity[21]. The charged multiplicity rises continually as the impact parameter decreases. However, the number of forward neutrons is largest at moderate impact parameters. In very central collisions, most of the nucleus interacts, leaving few remnant neutrons, while in very peripheral collisions, some of the nucleus remains intact, reducing the number of forward neutrons, producing the curve in Fig. 3.

5. Thermal Freezeout

The particles present at thermal freezeout are those observed in the RHIC detectors, and are relevant for comparison with models of heavy ion collisions. The charged particle multiplicity is shown as a function of pseudorapidity η in Fig. 4. The multiplicity $dN/d\eta$ is roughly flat for $|\eta| < 2$. This central plateau shows that there is boost invariance. Within this region, the system appears invariant with respect to the longitudinal boost (velocity); the expansion may be treated in 2 dimensions.

At 130 GeV, the maximum $dN/d\eta$ is about 570, rising to 650 at 200 GeV. This corresponds to total multiplicities of about 4100 ± 210 and 4960 ± 250 respectively[22]. These multiplicities are considerably lower than most pre-RHIC predictions[23], and seem to be best fit by models based on a combination of hard interactions (calculated by perturbative QCD) and soft interactions (extrapolated from lower energies). Most popular cosmic ray air shower codes predict considerably larger multiplicities[24].

The dN/dy per participant (nucleon involved in the collision) are about 40% higher than at lower energies, and also 50% higher than in $\overline{p}p$ collisions

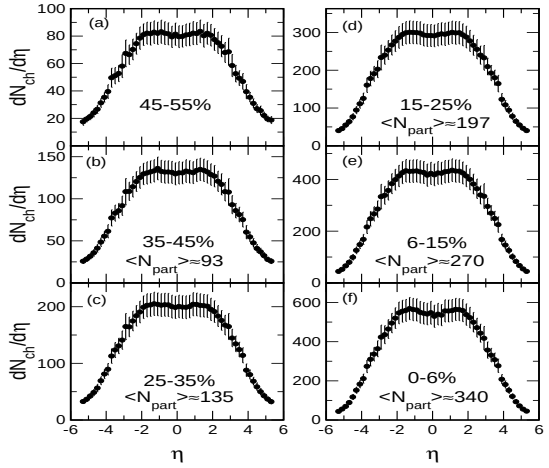

Figure 4. Charged multiplicity $dN/d\eta$ for different centrality bins at 130 GeV. A flat plateau is visible at mid-rapidity. From the PHOBOS collaboration[25].

at comparable energies[25]. The multiplicity per participant rises smoothly as the number of participants increases.

The PHENIX collaboration measured a transverse energy $dE_T/d\eta \approx 578$ GeV per unit η for the 2% most central collisions. This is the energy released in the collision. In a boost-invariant picture (supported by the existence of a central plateau), particles emitted into a pseudorapidity region $\delta\eta$ cine from a region of longitudinal size $\delta\eta c\tau$, where $\tau \approx \hbar/p_0$ is the time required for the initial interactions to occur. Here, p_0 is the energy scale for the initial particle production. The initial energy density depends on this scale. We will use a conservative $p_0 = 200$ MeV/c, so $\tau \approx 1$ fm/c. The initial volume is $\pi R_A^2 \delta\eta\tau$ and the energy density ϵ is

$$\epsilon \approx \frac{1}{\pi R_A^2 \tau}\frac{dE_T}{d\eta} \approx 4.5 \text{ GeV/fm}^3. \quad (1)$$

This is much larger than the 1 GeV/cm^3 that lattice gauge calculations predict is required to form a QGP. Although the time scale is not completely fixed, it seems hard to stretch τ enough to reduce ϵ below 1 GeV/cm^3.

The baryon:antibaryon ratio at freezeout is also of interest. Some baryons are initially present in the gold nuclei, while the rest are produced via baryon-antibaryon pair production. Antibaryons come only from the latter source. At 130 GeV, the $\overline{p} : p$ ratio is $0.6 \pm 0.02 \pm 0.06$, rising to 0.73 ± 0.03 for $\overline{\Lambda} : \Lambda$ and 0.82 ± 0.08 for $\overline{\Xi} : \Xi$ where the first (usually only) error is statistical[26].

These ratios are quite close to 1. The central region is nearly baryon free. Pair produced baryons outnumber initial state baryons by more than 2:1. However, the net baryon number is not zero, showing that there is indeed substantial baryon stopping; many initial state baryons are transported over 6 units of rapidity.

The size of the system at thermal freezeout has been measured with 2-particle interferometry (Hanbury-Brown Twiss interferometry), taking advantage of the Bose statistics that increase the abundance of particle pairs with momentum difference $\Delta p = p_1 - p_2 < \hbar/R$. Here R is the radius of the last elastic interaction. The momentum difference vector is decomposed into longitudinal (along the beam direction), side (transverse to the observer, and out (toward the observer) components (the Bertsch-Pratt decomposition). The source radius for a source with an assumed Gaussian is about 6 fermi in all 3 dimensions[27]. This is about twice the initial nuclear radius (about 6.5 fermi, in a Woods-Saxon [almost hard sphere] density distribution). This source size is similar to that observed in much lower energy collisions at the SPS; the lack of growth is a surprise. It is also surprising that the source radii in all 3 dimensions are similar; this indicates that the particles are emitted in a very short time scale, *i.e.* that thermal freezeout occurs quite suddenly over the entire nucleus.

Finally, we can compare the charged pion, proton and kaon spectra. For $p_T < 2$ GeV/c (the non-perturbative region), all three spectra are consistent with thermal emission. However, the three species have rather different apparent temperatures. The different temperatures may be due to a collective outward motion known as radial flow. If the expanding particles interact strongly, they tend to move outward at the same velocities. Then, the thermal fit temperature T_{app}

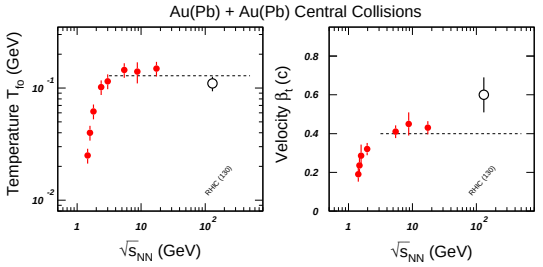

Figure 5. Temperatures T and expansion velocity β observed at different collision energies. From Ref. [28].

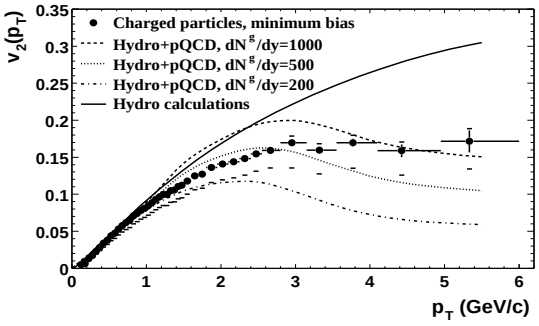

Figure 6. Elliptic flow (v_2) as a function of p_T. For $p_T < 2$ GeV/c, hydrodynamic models fit the data well. At higher energies, hydrodynamic models fail, as expected, and a parton description may be more appropriate. The data indicate that very high parton (mostly gluon) densities are required to produce the observed flow. From the STAR collaboration [31].

for a particle with mass m is

$$T_{app} = T + m\beta^2 \tag{2}$$

where T is the actual temperature and $\beta \cdot c$ is the collective expansion velocity. The 3 species satisfy Eq. 2 for $T = 120$ MeV and $\beta = 0.52$[28]. The system expands outward at more than half the speed of light! As Fig. 5 shows, the temperature is slightly lower than that measured at the SPS, but β is significantly higher. The temperature is comparable to the transition temperature predicted by LGT calculations. The very large β is characteristic of explosive expansion, with very high pressures and strong rescattering.

Anisotropic flow is another observable. In a non-central collision, the reaction zone is elliptical. Pressure converts this spatial asymmetry into a particle density/momentum anisotropy which is usually parameterized as

$$\frac{dN}{d\phi} = 1 + 2v_2 \cos(2\phi) \tag{3}$$

where ϕ the angle between the particle and the reaction plane (impact parameter vector), and v_2 is the elliptic flow. A large v_2 indicates high pressures and early equilibration[29]. Figure 6 shows the elliptic flow as a function of centrality, here given in terms of N_{ch}/N_{max}, where N_{ch} is the charged particle multiplicity relative to the maximum multiplicity N_{max}. The flow is large, and is very close to the predictions of hydrodynamic models that treat the system as a fluid. Flow has been studied for identified pions, protons and kaons ($K^{\pm}$ and K_s), and Λ. The p_T dependence of these species flow matches the predictions of hydrodynamic models quite well[30]. This fluid-like behavior is another indication of a strongly interacting system.

6. Chemical Freezeout

A key observable of chemical freezeout are the abundances of various particles. If the system is in chemical equilibrium, the abundances should scale as $\exp(-[\sqrt{m^2 + p_T^2} + \mu]/kT)$, where m is the particle mass, μ is the chemical potential of the particle (due to it's baryon and strangeness content), k is Boltzmann's constant, and T is the temperature[28]. Figure 7 compares the ratios of a number of different particles, compared with the thermal model predictions. The fit finds temperature $T = 187 \pm 8$ MeV, baryochemical potential $\mu_b = 39 \pm 4$ MeV, strange chemical potential $\mu_s = 1.8 \pm 1.6$ MeV, and strangeness suppression factor $\gamma_s = 1.00 \pm 0.05$. This is hotter than at thermal freezeout, which is a later, cooler stage

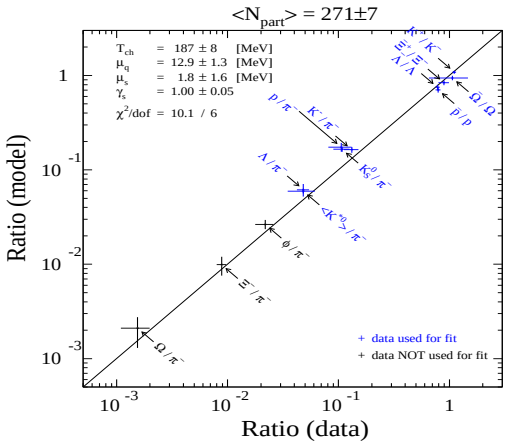

Figure 7. Measured particle multiplicity ratios vs. the results of a chemical fit model for the 6% most central gold-gold collisions at 130 GeV. The model axis errors are the uncertainties in the fit output[32].

in the evolution of the system. The μ_b is much less than the proton mass, showing quantitatively that the central region is effectively net baryon free.

The chemical equilibration of hadrons containing up, down and strange quarks ($\gamma_s = 1$) is very different from the situation in e^+e^-, pp and $p\overline{p}$ collisions. In these elementary collisions, $\gamma_s \approx 0.3$; strange hadrons are suppressed by a factor of 3 below the equilibrium expectations.

This strangeness equilibration was long-ago proposed as a signature of the quark-gluon plasma. In a QGP, reactions proceed quickly, and equilibrium should be reached rapidly. Reactions are much slower in a hadron gas and there are many species to produce, so equilibration takes much longer. Most (but not all) calculations indicate that the hadron gas equilibration takes much longer than the expected system lifetime[5].

7. Initial States/High p_T Particles

Study of the evolution of the system before chemical freezeout requires a probe particle that is created early in the collision. A few probes, such as direct photons escape the medium without interacting, and provide information about the process that created them. Others, such as charmonium and high p_T particles, interact with the medium and can provide information about how it evolves. These probes come from the hadronization of high p_T quarks and gluons (partons). As of this conference, RHIC has so far only presented results on the high p_T hadrons.

High p_T partons are produced very early in the collision, at a time $\tau \approx \hbar/p_T$. The partons are not expected to hadronize until much later, around a time $t = \hbar/\Lambda$, where $\Lambda \approx 300$ MeV is the typical QCD scale. Usually, the partons will have exited the medium before this point, so that hadronization occurs in free space. The medium will interact with the produced parton, not the final state hadrons. Since the final state hadron momenta depends on the parton momentum, any energy loss by the parton in the medium will be reflected in the high p_T hadron spectrum.

The parton energy loss can be studied by comparing hadron momentum spectra from central heavy ion collisions with spectra from peripheral heavy ion collisions and pp collisions. Published results, using the 130 GeV data, have used a pp reference spectrum derived from 200 GeV $p\overline{p}$ collision data from the UA1 experiment.

Fig. 8[33], compares charged hadron and π^0 production in central gold-gold collisions with a normalized pp spectrum. R_{AA} is the cross section ratio for gold-gold to pp collisions, divided by the number of nucleon-nucleon collisions in the gold. In the absence of nuclear effects, $R_{AA} = 1$. At low p_T soft (non-perturbative) physics is expected to dominate, leading to $R_{AA} \ll 1$, as observed. However, at higher p_T, where perturbative QCD applies well, we expect $R_{AA} = 1$. In contrast, at high p_T, in the data, R_{AA} flattens out at about 0.5 for charged hadrons, and 0.3 for π^0.

Nuclear effects, such as shadowing, multiple scattering and the net isospin difference can affect R_{AA}. In AA collisions, the incident nucleons may undergo soft interactions and acquire some initial state p_T before undergoing a hard interaction. Known as the Cronin effect, this initial-state p_T may increase the final state p_T and hence

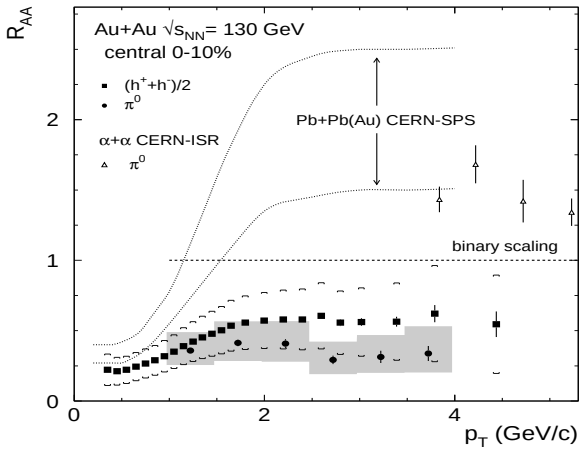

Figure 8. Comparison of charged hadron and π^0 p_T spectra from gold-gold collisions and a *pp* derived reference. From the PHENIX collaboration[33].

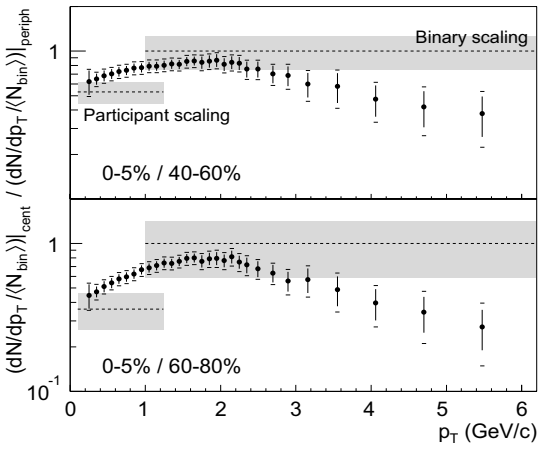

Figure 9. Comparison of the charged hadron p_T spectra from central and peripheral gold-gold collisions at 130 GeV. From the STAR collaboration[35].

the measured R_{AA}. Fig. 8 also shows R_{AA} from lead-lead collisions at a center of mass energy of 17 GeV/nucleon. There, for $p_T > 2$ GeV, R_{AA} rises considerably above 1. This is dramatically different from RHIC, showing a significant effect of the higher energy. In fact, the lower energy data shows no energy loss, while the RHIC data seems to indicate a very large energy loss[34].

The systematic errors in normalizing the UA1 and RHIC data vary with the particle momentum, but are in the 35% range, due to uncertainties in luminosities, cross sections, centrality selection, pseudorapidity distribution, etc. Figure 9 compares charged hadron spectra from peripheral and central gold-gold collisions[35]; R_A, the ratio of hard particle production in central and peripheral AA collisions, per nucleon-nucleon collision, is always less than 1. At high p_T, $R_A \approx 0.3$. The systematic uncertainties in R_A are about 20%.

More can be learned about hard interactions by considering correlations of high-p_T particles. The STAR collaboration has studied the angular correlations between particles with $p_T > 4$ GeV/c and $|\eta| < 0.7$ (the trigger particle) and a second particle with $p_T > 2$ GeV/c [36]. Figure 10 shows the azimuthal correlations, as a function of the azimuthal separation $\Delta\phi$. There is an enhancement near $\Delta\phi = 0$. This correlation has a similar strength and width in *pp* and AA collisions.

However, at large separations, $\Delta\phi \approx \pi$, no correlation is observed in the AA data, while a correlation is seen in the *pp* data. The back-to-back correlations in *pp* collisions are expected because jets are usually produced in back-to-back pairs known (although many of the produced jets may be outside the experimental acceptance). The correlations observed in the *pp* collisions match the theoretical expectations, but the jet pair correlations are absent in the AA data

The major difference expected between *pp* and AA collisions is anisotropic flow; the solid curve in Fig. 10 shows the size of the flow contribution. Flow cannot explain the difference between the *pp* and AA curves.

The suppression of high p_T particles, presence of same-side particle correlations and disappearance of opposite side particle correlations are all consistent with a strongly interacting system. Only partons produced near the surface of the system are able to escape and produce jets. When

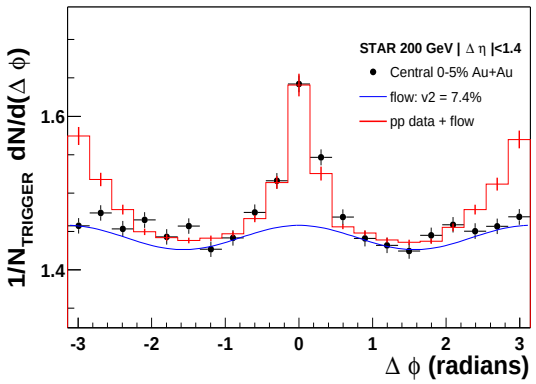

Figure 10. Correlation function for two high-p_T particles. The points are the 5% most central (smallest impact parameter) 200 GeV gold-gold collisions, while the histogram is 200 GeV pp data, both from the STAR detector[36].

a parton reaction produces back-to-back partons near the system surface, one parton escapes, almost unmodified, producing a jet. The other parton goes in the other direction, into the system, where it is absorbed. The large flow at high p_T (Fig. 6) supports this picture, showing that even energetic particles demonstrate collective effects.

8. Implications for Air Shower Simulations

This RHIC data can be used to test air shower simulations. As several people at the conference pointed out, the overall charged multiplicities are considerably lower than most predictions, including several popular air shower codes. Models based on separate hard (described by QCD) and soft (phenomenological) models seem to work best.

Gluon saturation models, which can affect the depth of maximum shower development, and the muon content of showers with energies above 10^{17} eV[37] are disfavored, but not ruled out. In these models, the gluon density in heavy ions becomes saturated, and low$-x$ gluons may recombine, reducing their abundance. They predict that the charged particle multiplicity in AA collisions should be lower than the multiplicity scaled from pp collisions; data shows the opposite, with the AA multiplicity higher than in simple pp scaling.

Several other effects are likely to be relevant for air showers. Strange particles are copiously produced, in chemical equilibrium. This might affect the muon content of air showers, compared to expectations for pp collisions.

The presence of non-zero net baryon density at mid-rapidity shows that there is a substantial amount of baryon stopping, even at very high energies. In a fixed target frame of reference, these baryons carry enormous energy, and so this stopping may have implications for the overall energy flow in the collision.

Several very different analyses show that the colliding system interacts very strongly, exhibiting collective behavior that suppresses high p_T particle production. Pure-QCD calculations that neglect collective effects may over-predict the number of high p_T particles, and hence the shower density far from the core.

The existing RHIC data is for gold on gold collisions, not the lighter ions and protons found in cosmic rays and the atmosphere. Interpolation between pp and gold-gold collisions is not easy. In the next few years, RHIC will collide lighter ions; until then, the various Monte Carlo codes can only be tested with light (proton) or heavy (gold) systems.

9. Conclusions

RHIC is just beginning it's study of ultra-relativistic heavy ion collisions. However, already we see a few surprises: large elliptic flow, suppression of high p_T particles, and the complete chemical equilibration of strange particles. Chemical and thermal equilibrium appear to have been reached. This data shows that the system interacts strongly and appears to equilibrate early in the collision.

But, is this the quark-gluon plasma? The evidence suggests that the high densities are strong interactions are consistent with a quark-gluon plasma. However, a very high density hadron gas cannot yet be ruled out.

I would like to thank the STAR, PHOBOS, BRAHMS and PHENIX collaborations for making their data and plots available to me. This work was funded by the U.S. Dept. of Energy under contract DE-AC-03-76SF00098.

REFERENCES

[1] P. Senger and H. Ströebele, J. Phys. G**25**, R59 (1999).
[2] W. Reisdorf and H. G. Ritter, Ann. Rev. Nucl. Part. Sci. **47**, 663 (1997).
[3] S. A. Bass *et al.*, J. Phys. G**25**, R1 (1999).
[4] S. Margetis, K. Safarik and O. Villalobos Baillie, Ann. Rev. Nucl. Part. Sci. **50**, 299 (2000).
[5] P. Koch, B. Müller and J. Rafelski, Phys. Re. **142**, 167 (1986).
[6] R. Vogt, Phys. Rep. **310**, 197 (1999).
[7] W. Guryn, Nucl. Phys. B (Proc. Suppl.) **99**, 299 (2001).
[8] See http://www.phenix.bnl.gov/.
[9] See http://www.star.bnl.gov/.
[10] See http://www.phenix.bnl.gov/.
[11] See http://www.phenix.bnl.gov/.
[12] C. Adler *et al.*, Nucl. Instrum. & Meth. **A461**, 337 (2001).
[13] G. Baur, K. Hencken, D. Trautmann, S. Sadovsky and Y. Kharlov, Phys. Rep. **364**, 359 (2002); F. Krauss, M. Greiner and G. Soff, Prog. Part. Nucl. Phys. **39**, 503 (1997).
[14] S. Klein and J. Nystrand, Phys. Rev. Lett. **84**, 2330 (2000).
[15] S. Klein, J. Nystrand and R. Vogt, Phys. Rev. **C66**, 044906 (2002).
[16] L. Frankfurt, M. Strikman and M.Zhalov, Phys. Lett. **B540**, 220 (2002).
[17] A. J. Baltz, C. Chasman and S. N. White, Nucl. Instrum & Meth. **A417**, 1 (1998); M. Chiu *et al.*, Phys. Rev. Lett. **89**, 012302 (2002).
[18] C. Adler *et al.* (STAR Collaboration), nucl-ex 0206004.
[19] S. Klein and J. Nystrand, Phys. Rev. **C60**, 014903 (1999); A. Baltz, S. Klein and J. Nystrand, Phys. Rev. Lett. **89**, 012301 (2002).
[20] H. Satz, Rept. Prog. Phys. **63**, 1511 (2000).
[21] K. Adcox *et al.* (PHENIX Collaboration), Phys. Rev. Lett. **86**, 3500 (2001).
[22] W. Busza, presented at the workshop on "QCD in the RHIC Era," April 8-12, 2002, Santa Barbara, CA.
[23] K. J. Eskola, Nucl. Phys. **A698**, 78c (2002).
[24] R. Engel, these proceedings.
[25] B. B. Back *et al.* (PHOBOS Collaboration), Phys. Rev. Lett. **87**, 102303 (2001).
[26] H. Caines, for the STAR Collaboration, Nucl. Phys. **A698**, 112c (2002).
[27] C. Adler *et al.*, (STAR Collaboration), Phys. Rev. Lett. **87**, 082301 (2001); K. Adcox *et al.*, (PHENIX Collaboration), Phys. Rev. Lett. **88**, 192302 (2002).
[28] N. Xu and M. Kaneta, Nucl. Phys. **A698**, 306c (2002).
[29] K. H. Ackermann *et al.* (STAR Collaboration), Phys. Rev. Lett. **86**, 402 (2001); K. Adcox *et al.*, (PHENIX Collaboration), nucl-ex/0204005; B. B. Back *et al.*, (PHOBOS Collaboration), nucl-ex/0205021.
[30] C. Adler *et al.* (STAR Collaboration), Phys. Rev. Lett. **87**, 182301 (2001); C. Adler *et al.*, (STAR Collaboration) Phys. Rev. Lett. **89**, 132301 (2002).
[31] C. Adler *et al.* (STAR Collaboration), nucl-ex/0206006.
[32] N. Xu and M. Kaneta, private communication. The figure is updated from Fig. 7 of Ref. [28].
[33] C. Adcox *et al.* (PHENIX Collaboration), Phys. Rev. Lett. **88**, 022301 (2002); C. Adcox *et al.* (PHENIX Collaboration), nucl-ex/0207009.
[34] X. N. Wang, presented at the workshop on "QCD in the RHIC Era," April 8-12, 2002, Santa Barbara, CA.
[35] C. Adler *et al.* (STAR Collaboration), nucl-ex/0206011.
[36] C. Adler *et al.* (STAR Collaboration), nucl-ex/0210033.
[37] C. Pajares, D. Sousa and R. A. Vazquez, Phys. Rev. Lett. **86**, 1674 (2001).